Epithelial Gpr116 regulates pulmonary alveolar homeostasis via G$_{q/11}$ signaling

Kari Brown, … , Jeffrey A. Whitsett, James P. Bridges

Research Article   Cell biology   Pulmonology

Pulmonary function is dependent upon the precise regulation of alveolar surfactant. Alterations in pulmonary surfactant concentrations or function impair ventilation and cause tissue injury. Identification of the molecular pathways that sense and regulate endogenous alveolar surfactant concentrations, coupled with the ability to pharmacologically modulate them both positively and negatively, would be a major therapeutic advance for patients with acute and chronic lung diseases caused by disruption of surfactant homeostasis. The orphan adhesion GPCR GPR116 (also known as Adgrf5) is a critical regulator of alveolar surfactant concentrations. Here, we show that human and mouse GPR116 control surfactant secretion and reuptake in alveolar type II (AT2) cells by regulating guanine nucleotide–binding domain α q and 11 (G$_{q/11}$) signaling. Synthetic peptides derived from the ectodomain of GPR116 activated G$_{q/11}$-dependent inositol phosphate conversion, calcium mobilization, and cortical F-actin stabilization to inhibit surfactant secretion. AT2 cell–specific deletion of *Gnaq* and *Gna11* phenocopied the accumulation of surfactant observed in *Gpr116$^{-/-}$* mice. These data provide proof of concept that GPR116 is a plausible therapeutic target to modulate endogenous alveolar surfactant pools to treat pulmonary diseases associated with surfactant dysfunction.

Find the latest version:

https://jci.me/93700/pdf

Epithelial Gpr116 regulates pulmonary alveolar homeostasis via $G_{q/11}$ signaling

Kari Brown,[1] Alyssa Filuta,[1] Marie-Gabrielle Ludwig,[2] Klaus Seuwen,[2] Julian Jaros,[2] Solange Vidal,[2] Kavisha Arora,[3] Anjaparavanda P. Naren,[3] Kathirvel Kandasamy,[4] Kaushik Parthasarathi,[4] Stefan Offermanns,[5] Robert J. Mason,[6] William E. Miller,[7] Jeffrey A. Whitsett,[1] and James P. Bridges[1]

[1]Department of Pediatrics, Perinatal Institute, Section of Pulmonary Biology, Cincinnati Children's Hospital Medical Center, Cincinnati, Ohio, USA. [2]Novartis Institutes for Biomedical Research, Basel, Switzerland. [3]Department of Pediatrics, Division of Pulmonary Medicine, Cincinnati Children's Hospital Medical Center, Cincinnati, Ohio, USA. [4]Department of Physiology, University of Tennessee Health Sciences Center, Memphis, Tennessee, USA. [5]Department of Pharmacology, Max Planck Institute for Heart and Lung Research, Bad Nauheim, Germany. [6]Department of Medicine, National Jewish Health, Denver, Colorado, USA. [7]Department of Molecular Genetics, University of Cincinnati College of Medicine, Cincinnati, Ohio, USA.

Pulmonary function is dependent upon the precise regulation of alveolar surfactant. Alterations in pulmonary surfactant concentrations or function impair ventilation and cause tissue injury. Identification of the molecular pathways that sense and regulate endogenous alveolar surfactant concentrations, coupled with the ability to pharmacologically modulate them both positively and negatively, would be a major therapeutic advance for patients with acute and chronic lung diseases caused by disruption of surfactant homeostasis. The orphan adhesion GPCR GPR116 (also known as Adgrf5) is a critical regulator of alveolar surfactant concentrations. Here, we show that human and mouse GPR116 control surfactant secretion and reuptake in alveolar type II (AT2) cells by regulating guanine nucleotide–binding domain α q and 11 ($G_{q/11}$) signaling. Synthetic peptides derived from the ectodomain of GPR116 activated $G_{q/11}$-dependent inositol phosphate conversion, calcium mobilization, and cortical F-actin stabilization to inhibit surfactant secretion. AT2 cell–specific deletion of *Gnaq* and *Gna11* phenocopied the accumulation of surfactant observed in *Gpr116*^{−/−} mice. These data provide proof of concept that GPR116 is a plausible therapeutic target to modulate endogenous alveolar surfactant pools to treat pulmonary diseases associated with surfactant dysfunction.

Introduction

Pulmonary surfactant, synthesized by alveolar type II (AT2) epithelial cells in the alveoli, is a lipid-protein complex that reduces surface tension at the air-liquid interface, preventing atelectasis during the respiratory cycle. Following synthesis, phospholipids and surfactant proteins B and C are routed to and stored in membrane-enclosed secretory organelles termed lamellar bodies. Stimulation by secretagogues (including purines, refs. 1, 2; β-agonists, refs. 3–5; and adenosine, refs. 6, 7) or mechanical stretching of AT2 cells (8) causes fusion of lamellar bodies with the plasma membrane and their exocytosis into alveolar spaces.

Surfactant concentrations increase in late gestation to facilitate the transition to air breathing at birth. Following the fetal-to-neonatal transition, surfactant pool sizes decline, mediated by decreased secretion and increased catabolism, and are maintained at lower levels throughout adulthood (9–11). In the adult lung, alveolar surfactant pool sizes are tightly regulated and maintained through the balance of synthesis, secretion, and recycling by AT2 cells and by uptake and catabolism by alveolar macrophages (12). Perturbations in surfactant concentrations or composition due to prematurity, pulmonary infections, or mutations in genes critical for surfactant homeostasis are associated with acute and chronic lung diseases in children and adults.

GPCRs comprise the largest class of cell membrane receptors, with much of vertebrate physiology being influenced by GPCR signal transduction. Three GPCR-mediated pathways were implicated in surfactant secretion by AT2 cells: purinergic receptor P2Y (*P2ry2*), β$_2$ adrenergic receptor (*Adrb2*), and adenosine A$_{2B}$ receptors (*Adora2b*) (1–6). Activation of GPCRs by their cognate agonists in AT2 cells causes increased cytosolic levels of second messengers, including IP3, DAG, (Ca2+)$_i$, or cAMP, that activate PKC, PKA,

and/or Ca^{2+}/calmodulin-dependent protein kinase to enhance surfactant secretion (13–16). Mechanical stretch induces surfactant secretion via ATP- and Ca^{2+}-dependent pathways (8, 17–20). While G protein signaling was implicated in surfactant secretion in vitro, mechanisms by which individual GPCRs regulate surfactant homeostasis remain incompletely understood. For example, $P2ry2^{-/-}$, $Adora2b^{-/-}$, and $Adrb2^{-/-}$ mice are viable without a reported surfactant phenotype (21–23).

GPR116 (also known as Adgrf5) is a member of the adhesion class of GPCRs (AdGPCRs), which share extracellular domains containing highly conserved GPCR autoproteolysis–inducing (GAIN) domains. During synthesis of GPR116, intracellular autoproteolytic processing of nascent GPR116 proteins within the GAIN domain generates a mature protein, consisting of an N-terminal fragment (NTF) that is noncovalently linked to the C-terminal fragment (CTF), consisting of a 7 transmembrane (7TM) domain and a cytoplasmic domain (24). Mature GPR116 is routed to the plasma membrane where the NTF and CTF remain associated. GPR116 and the majority of AdGPCRs are orphan receptors; however, ligands have been identified for 9 of the 33 members and are primarily extracellular matrix proteins (25). Several full-length adhesion GPCRs, including GPR56, GPR64, GPR114, GPR126, and GPR133, show G protein–coupled signaling, and expression of mutants lacking the extracellular NTF augments basal G protein activity (26–30). The ectodomain regions of AdGPCR CTF, from the GPS cleavage site to the first transmembrane domain, function as tethered peptides that activate G protein signaling through interactions with the 7TM domains. Synthetic peptides corresponding to CTF ectodomain sequences activate G protein–coupled responses downstream of the full-length receptors for several adhesion GPCRs (27, 28, 31, 32).

In the lung, GPR116 is localized to the plasma membrane of alveolar type I (AT1) and AT2 cells and *Gpr116* RNA is detected in pulmonary endothelial cells (33, 34). While previous data demonstrate the critical role of GPR116 in the regulation of pulmonary surfactant homeostasis and lung function, as exemplified by alveolar surfactant overload and parenchymal tissue simplification/destruction in $Gpr116^{-/-}$ mice (33–37), its mechanisms of action to regulate surfactant secretion are unclear. In the present study, we demonstrate that GPR116 is activated by its extracellular domain to activate GNAQ/GNA11, in turn regulating secretion of pulmonary surfactant.

Results

GPR116 regulates surfactant secretion and uptake in AT2 cells. Epithelial deletion of *Gpr116* (mediated by *Shh*-Cre), but not endothelial deletion of *Gpr116* (mediated by *Tie2*Cre), largely phenocopied the surfactant accumulation phenotype of $Gpr116^{-/-}$ mice (Figure 1A). The *Shh*Cre allele (38) causes recombination in both AT1 and AT2 epithelial cells due to expression in the developing lung endoderm prior to AT1 and AT2 differentiation. To definitively test the role of AT2 cell GPR116, we generated AT2 cell–specific *Gpr116* loss-of-function mice by mating $Gpr116^{f/f}$ mice with tamoxifen-inducible *Sftpc*CreER mice (39). Exposure of 4-week-old *Sftpc*CreER:$Gpr116^{f/f}$ mice to tamoxifen for 7 days caused a 4-fold increase in saturated phosphatidylcholine (SatPC) in bronchoalveolar lavage fluid (BALF), demonstrating that AT2 cell–specific expression of GPR116 is critical for surfactant homeostasis (Figure 1A). Since P2RY2 expression was increased in $Gpr116^{-/-}$ AT2 cells (33) and P2RY2 pathway activation stimulates surfactant secretion in isolated cells, we assessed surfactant pools in $P2ry2^{-/-}$:$Gpr116^{-/-}$ mice. Surfactant levels in $P2ry2^{-/-}$:$Gpr116^{-/-}$ mice were similar to $Gpr116^{-/-}$ mice, indicating that P2RY2 is dispensable in the context of GPR116-dependent surfactant dysregulation (Supplemental Figure 1; supplemental material available online with this article; https://doi.org/10.1172/jci.insight.93700DS1).

To test whether surfactant accumulation was caused by increased secretion or decreased uptake by AT2 cells, we performed phospholipid secretion and surfactant uptake assays in primary $Gpr116^{-/-}$ AT2 cells. As shown in Figure 1B, constitutive secretion of isotope-labeled surfactant phospholipids was significantly increased (1.7-fold) in $Gpr116^{-/-}$ AT2 cells. Likewise, ATP-induced secretion was increased 1.8-fold (Figure 1C). To determine if surfactant uptake was defective in $Gpr116^{-/-}$ AT2 cells, surfactant uptake studies were performed in primary cells. Uptake of surfactant was significantly impaired in $Gpr116^{-/-}$ AT2 cells (Figure 1D). Collectively these data demonstrate that GPR116 controls surfactant homeostasis via modulation of both surfactant secretion and uptake by AT2 cells.
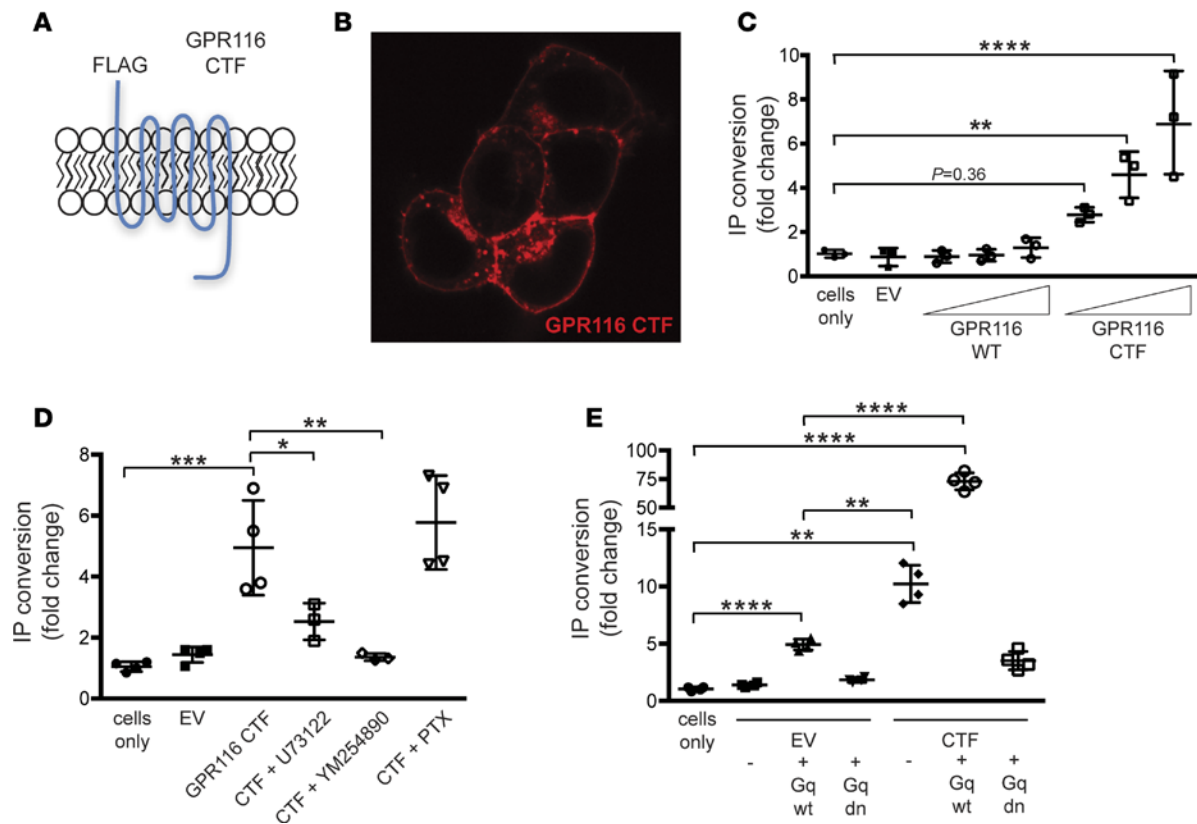
GPR116 CTF activates $G_{q/11}$ signaling. To determine if heterologous expression of mouse GPR116 (mGPR116) elicits $G_{q/11}$-coupled responses, we generated FLAG-tagged GPR116 and GPR116 CTF domain constructs (Figure 2A). Transfection of GPR116 CTF in HEK293 cells resulted in prominent cell surface expression (Figure 2B and Supplemental Figure 2), causing dose-dependent accumulation of
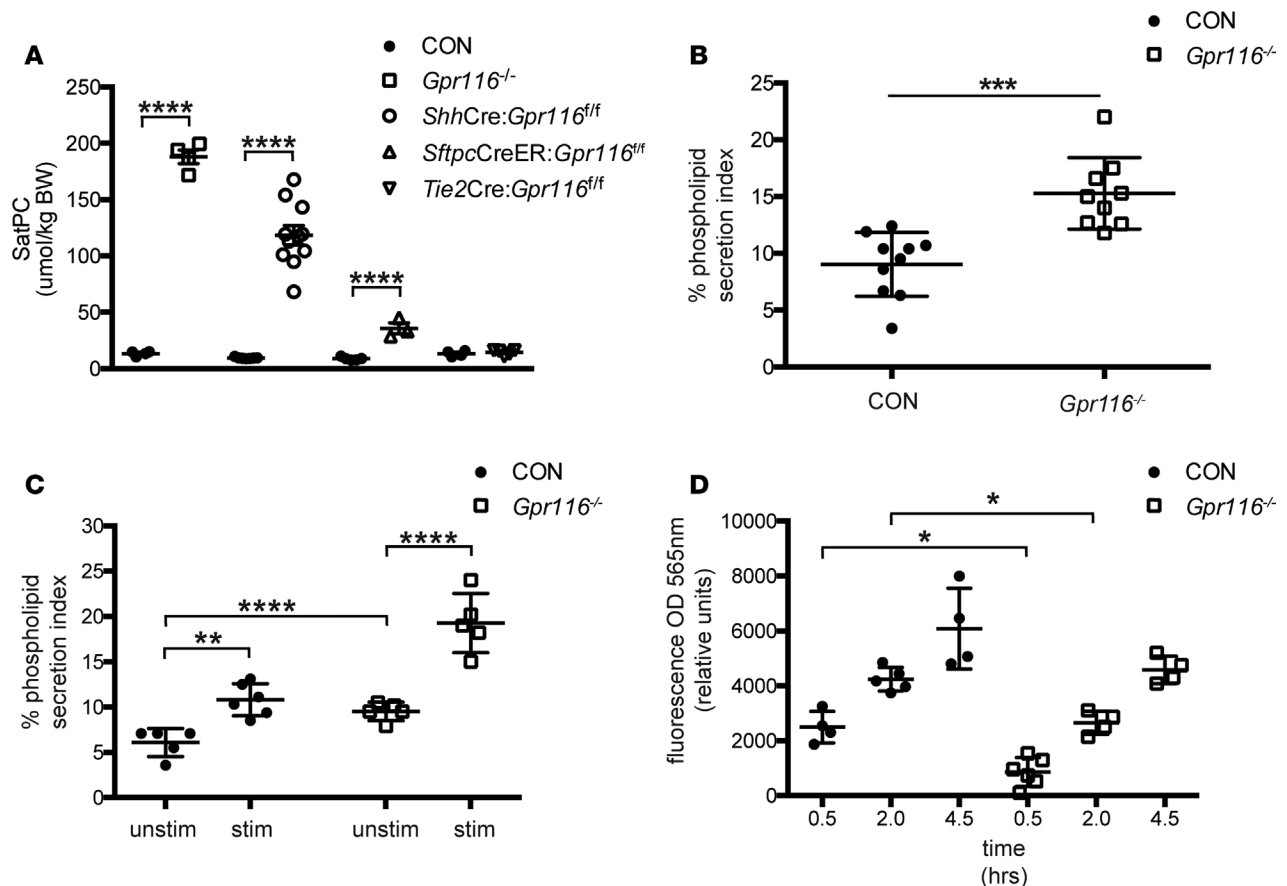
Figure 1. Epithelial deletion of GPR116 alters surfactant homeostasis in mice. (**A**) Saturated phosphatidylcholine (SatPC) levels in bronchoalveolar lavage fluid from 4-week-old $Gpr116^{-/-}$ mice, epithelial-specific GPR116 loss-of-function mice (ShhCre:$Gpr116^{f/f}$), AT2 cell–specific GPR116 loss-of-function mice ($Sftpc$CreER:$Gpr116^{f/f}$), endothelial-specific GPR116 loss-of-function mice ($Tie2$Cre:$Gpr116^{f/f}$), and control mice (CON, littermate controls for each genotype). $Sftpc$CreER:$Gpr116^{f/f}$ mice were placed on tamoxifen chow for 7 days. Data represent 3 independent experiments, with n = 3–4 mice per group. (**B**) In vitro basal phospholipid secretion assays of primary WT and $Gpr116^{-/-}$ AT2 cells. Secretion was measured as SatPC content in media after a 3-hour incubation time divided by SatPC content in cell lysate (n = 2 individual experiments, 2–3 biological replicates per group). (**C**) In vitro phospholipid secretion assays in the absence (unstim) and presence (stim) of ATP stimulation (n = 2 individual experiments, 2–3 biological replicates per group). (**D**) Surfactant uptake assays in primary CON and $Gpr116^{-/-}$ type II cells (n = 2 individual experiments, 2–3 biological replicates per group). Data are expressed as mean ± SD. *P < 0.05, **P < 0.01, ***P < 0.001, ****P < 0.0001 (1-way ANOVA for **A**, **C**, and **D**; unpaired t test for **B**).

inositol phosphate (IP), consistent with $G_{q/11}$ coupling (Figure 2C). Full-length GPR116 failed to induce IP accumulation, demonstrating its lack of constitutive $G_{q/11}$-dependent activity (Figure 2C). YM-254890, a $G_{q/11}$ inhibitor (40), inhibited and U73122, a phospholipase C inhibitor, significantly attenuated GPR116 CTF-dependent IP responses (Figure 2D). G protein β and γ protein subunits, liberated from the α subunit of GNAI following activation, have been shown to activate phospholipase C, resulting in IP3 accumulation (41). Pretreatment of GPR116 CTF-transfected cells with the GNAI inhibitor pertussis toxin had no effect on IP3 levels, demonstrating that IP3 responses in the context of GPR116 were independent of G protein β and γ subunit release from GNAI (Figure 2D). Coexpression of WT G_q or dominant-negative G_q (Q209L,D277N, ref. 42) enhanced or suppressed CTF-dependent IP conversion, respectively (Figure 2E). These data are consistent with $G_{q/11}$ activation by GPR116 CTF domain but not by full-length GPR116.
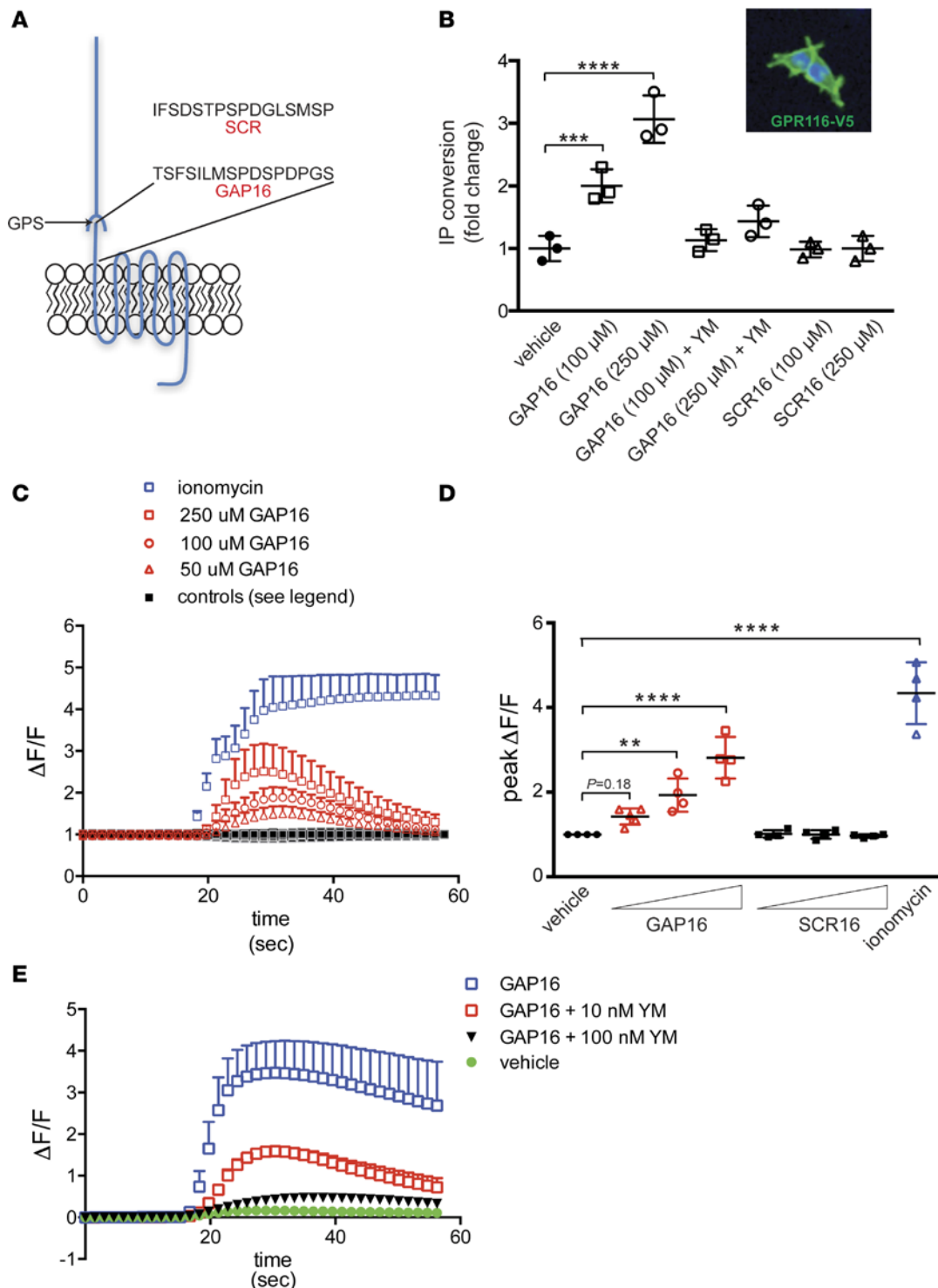
Peptide-induced activation of GPR116. The ligand(s) interacting with GPR116 is currently unknown. Constitutive activity of the CTF, coupled with lack of basal signaling from the full-length receptor, suggested that the NTF of GPR116 functions to inhibit CTF activity in the absence of ligand binding. This "tethered agonist" mode of activation, as occurs for protease-activated receptors, had been considered for the AdGPCR family and recently demonstrated for several AdGPCRs in cell culture and zebrafish models (27, 28, 31, 32). Since the ectodomain of GPR116 CTF is 100% conserved between mouse and rat and 93.8% conserved (15 of 16 amino acids) between mouse and human (Supplemental Figure 3A), we hypothesized that a peptide

Figure 2. GPR116 CTF activates G_{q/11} signaling. (**A**) Model of FLAG-tagged GPR116 CTF protein in plasma membrane. (**B**) Confocal image of GPR116 CTF-FLAG protein in HEK cells 12 hours after transfection. Original magnification, ×100. (**C–E**) Inositol phosphate (IP) conversion assays of HEK cells transiently transfected with empty vector (EV), GPR116 WT, or CTF plasmids. (**C**) CTF expression resulted in dose-dependent IP conversion (100 ng, 250 ng, 750 ng GPR116 CTF-FLAG plasmid/12-well plate; $n = 3$ independent experiments, 2 biological replicates per group). (**D**) Pretreatment with U73122 (10 μM) or YM-254890 (10 nM) 1 hour prior to assay attenuated or completely inhibited CTF-induced IP conversion, respectively; pretreatment with pertussis toxin (PTX, 100 ng/ml) 18 hours prior to assay had no effect on CTF-induced IP conversion ($n = 3$ independent experiments, 2 biological replicates per group). (**E**) Coexpression of EV or GPR116 CTF with WT Gnaq (Gq wt) or dominant-negative Gnaq (dn Gq; G209L,D277N) potentiated or inhibited CTF-induced IP conversion, respectively ($n = 3$ independent experiments, 2 biological replicates per group). Data are expressed as mean ± SD. *$P < 0.05$, **$P < 0.01$, ***$P < 0.001$, ****$P < 0.0001$ (1-way ANOVA for **C–E**).

identical to the sequence of the endogenous ectodomain of GPR116 CTF would activate GPR116. We synthesized a peptide consisting of the first 16 amino acids of the ectodomain of mGPR116 CTF, referred to hereafter as GAP16 (GPR116-activating peptide, 16 aa); a scrambled peptide (SCR) of equivalent amino acid composition was used as a control (Figure 3A). GAP16 treatment of HEK293 cells transiently expressing mGPR116-V5 caused a dose-dependent increase in IP conversion (Figure 3B). Cotreatment of cells with YM-254890 completely inhibited GAP16-induced IP conversion, demonstrating G_{q/11} coupling of activated GPR116. To identify additional G_{q/11}-mediated responses downstream of GPR116, calcium transient assays were performed in GPR116-expressing cells following GAP16 stimulation. GAP16 caused dose-dependent Ca^{2+} responses that were rapid and transient in nature (Figure 3, C and D), consistent with receptor-mediated signaling. Consistent with CTF IP conversion data (Figure 3B), YM-254890 blocked GAP16-dependent Ca^{2+} flux in a dose-dependent manner (Figure 3E). GAP16 neither caused cAMP accumulation nor inhibited forskolin-induced cAMP responses, consistent with the lack of GPR116 coupling to G_s or G_i proteins (Supplemental Figure 3B). These data demonstrate that a peptide (GAP16) corresponding to the CTF domain of GPR116 activates G_{q/11}-mediated responses in cells expressing GPR116.

GAP16 activates GPR116 in primary mouse AT2 cells. Imaging-based calcium transient assays were used to determine if GAP16 activates endogenous GPR116 in primary mouse AT2 cells. AT2 cells were cultured on a basement membrane/collagen mix that supports differentiation in culture (43). GAP16 stimulation of control AT2 cells caused rapid calcium flux, similar to that observed in heterologous expression assays (Figure 4, A–C; Supplemental Table 3; and Supplemental Videos 1 and 2). AT2 cells from *Gpr116^{-/-}* mice were unresponsive to GAP16, demonstrating GPR116 dependence of the GAP16-induced

Figure 3. Peptide-induced activation of GPR116. (**A**) Model of the full-length GPR116 protein with the GAP16 peptide corresponding to the amino acids of the CTF ectodomain and scrambled (SCR) peptide sequence. (**B**) Membrane localization of transfected V5-tagged GPR116 in HEK cells (inset, green = V5-tagged GPR116, blue = DAPI-stained nuclei; original magnification, ×60) and IP conversion assays. GAP16 treatment resulted in dose-dependent IP conversion that was inhibited by cotreatment with the Gq inhibitor YM-254890 (100 nM) (n = 3 independent experiments, 2 biological replicates per group). (**C**) Representative calcium transient traces of GAP16-stimulated GPR116-V5 stably transfected HEK cells. Ionomycin was added as a positive control; overlaying control lines in black include SCR peptide (50 μM, 100 μM, and 250 μM) and vehicle (n = 3 independent experiments, 3 biological replicates per group). (**D**) Quantification of calcium transient data (n = 4 independent experiments, 3 biological replicates per group). (**E**) Calcium transients of GAP16-stimulated (250 μM), GPR116-V5 stably transfected HEK cells pretreated with the G_q inhibitor YM-254890 (YM) 2 hours prior to stimulation (n = 3 independent experiments, 2 biological replicates per group). Data are expressed as mean ± SD. **P < 0.01, ***P < 0.001, ****P < 0.0001 (1-way ANOVA for **B** and **D**).
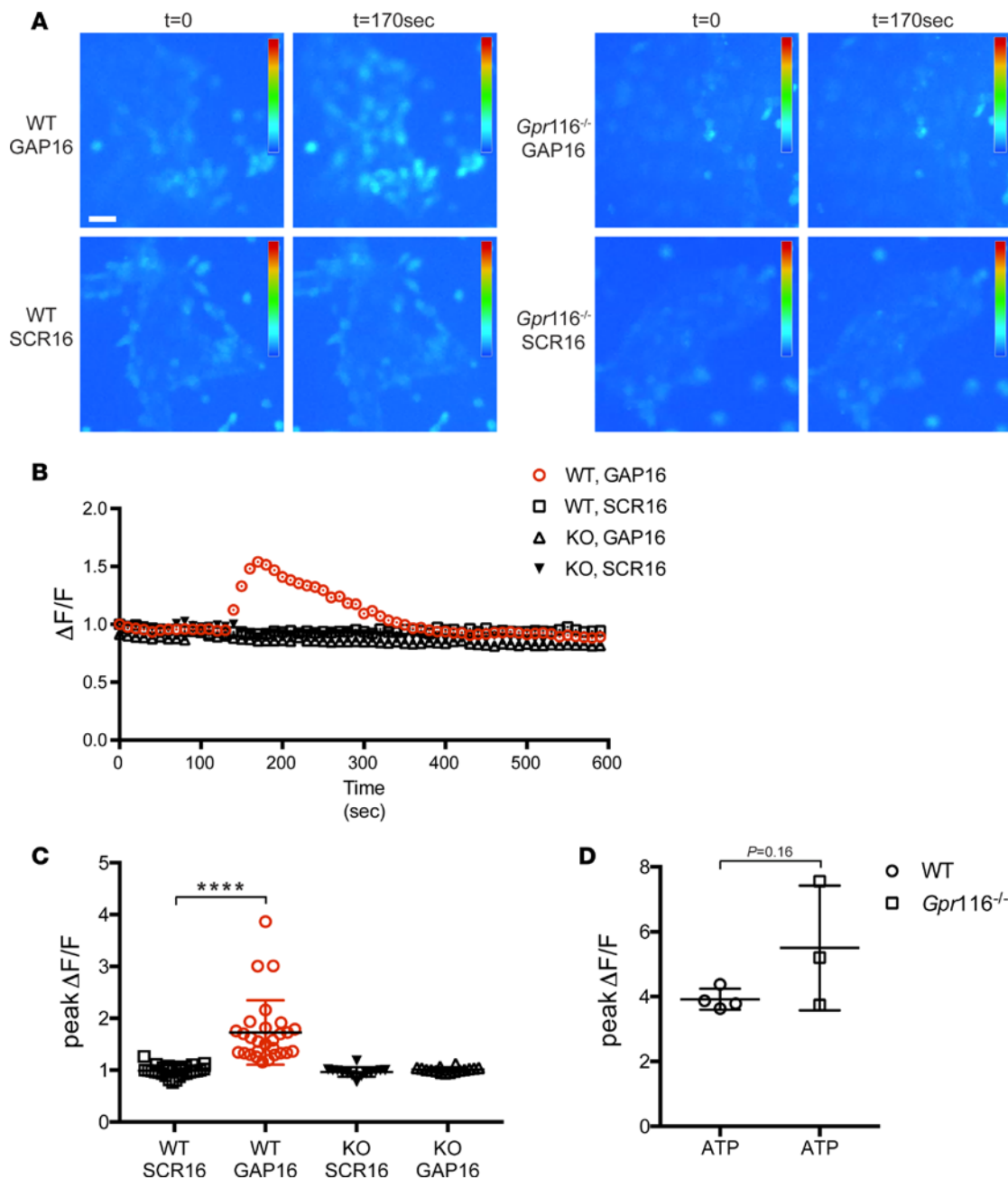
Figure 4. GAP16 activation of GPR116 in isolated mouse primary alveolar type II cells. Fluo-4 imaging–based calcium transient assays in adult WT and *Gpr116*^{-/-} primary mouse alveolar type II (AT2) cells. (**A**) GAP16 or SCR (250 μM) were added approximately 120 seconds after start of imaging. Representative images for WT and *Gpr116*^{-/-} cells at start of imaging and 170 seconds after peptide addition (scale bar: 10 μm for all images). Representative traces (**B**) and quantitation of peak calcium responses (**C**) from imaging data in WT or *Gpr116*^{-/-} adult primary mouse AT2 epithelial cells. Data represent 5 independent experiments for WT cells, 3 independent experiments for *Gpr116*^{-/-} cells, and 3 biological replicates per group. (**D**) Peak calcium responses in WT or *Gpr116*^{-/-} cells stimulated with ATP (50 μM). Data represent 1 experiment, 3–4 biological replicates per group. Data are expressed as mean ± SD. ****$P < 0.0001$ (1-way ANOVA for **C**, unpaired *t* test for **D**).

calcium response. *Gpr116*^{-/-} and control cells showed similar, albeit variable, calcium responses following stimulation with the *P2ry2*-agonist ATP, demonstrating that *Gpr116*^{-/-} AT2 cells are capable of eliciting $G_{q/11}$-coupled responses independent of GPR116 (Figure 4D). Collectively, these data demonstrate that GAP16 activates the endogenous GPR116 receptor in AT2 cells.

Identification of GPR116 CTF ectodomain amino acids required for receptor activation. Mutation analyses of the CTF ectodomain were undertaken to identify residues that conferred constitutive $G_{q/11}$ activity. The 15
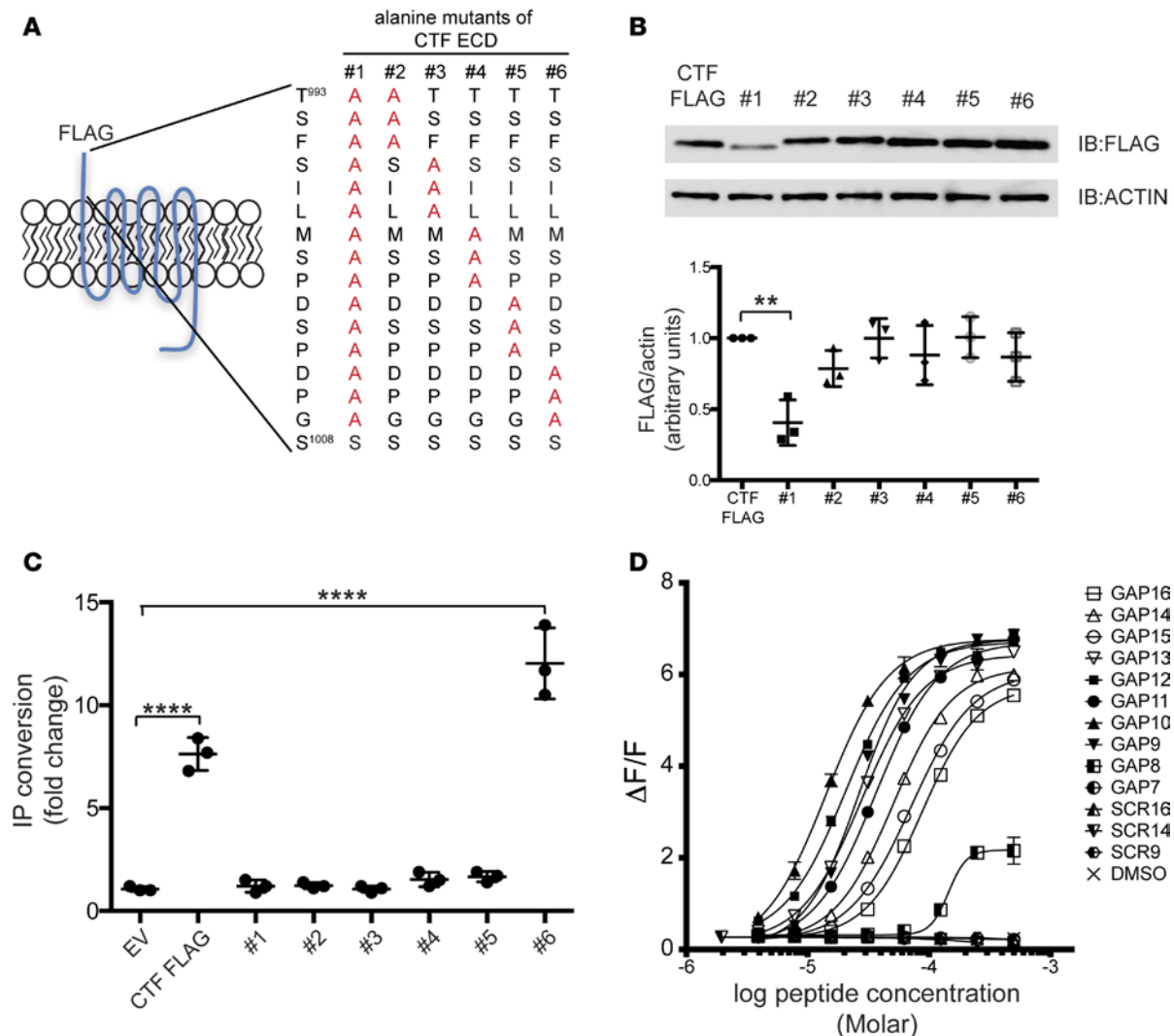
Figure 5. Characterization of GPR116 CTF ectodomain amino acids involved in receptor activation. (**A**) Diagram of amino acid residues in the ectodomain of GPR116 CTF and alanine mutant constructs generated to identify residues required for IP conversion activity. (**B**) Representative Western analysis of GPR116 CTF alanine mutants compared with WT GPR116-FLAG. The graph represents quantitative data of Western blot analyses for *n* = 3 experiments. (**C**) IP conversion assays in transiently transfected HEK cells. Data represent 4 independent experiments, 2 biological replicates per group. (**D**) Activity of truncated activating peptides. HEK cells stably expressing GPR116 (cell line 3C) were stimulated with GAP16 as a reference and C-terminally truncated peptides (GAP15-GAP7). A representative graph from 3 independent calcium transient experiments is shown; mean EC_{50} and control data are shown in Supplemental Figure 2. Data are expressed as mean ± SD. **$P < 0.01$, ****$P < 0.0001$ (1-way ANOVA for **B** and **C**).

amino acids immediately downstream of the GPS cleavage site, T993 to G1007, were mutated to alanine or changed in sequential steps of 3 amino acids (Figure 5A). All constructs, except the one in which all 15 amino acids were mutated to alanine, expressed at levels similar to those seen with the parental construct CTF FLAG (Figure 5B; see complete unedited blots in the supplemental material). IP conversion assays demonstrated lack of IP conversion for the T993A-F995A through the D1002A-P1004A mutants, while the D1005A-G1007A mutant was comparably active compared with the parental construct, demonstrating that amino acids T993 through P1004 of the CTF are critical for the activity of GPR116 (Figure 5C). To identify residues within the stimulating peptide required for GPR116 activation, we stimulated cells expressing full-length GPR116 with GAP16 and C-terminally truncated peptides (peptide sequences listed in Supplemental Table 1). GAP9 was identified as the minimal active peptide in calcium transient assays (Figure 5D). GAP10 was the most potent, suggesting an important role of the aspartic acid at position 10 (corresponding to D1002 in GPR116 CTF) for interaction with the 7TM domains. The relevance of these observations to human GPR116 (hGPR116) was demonstrated in HEK cells overexpressing hGPR116. GAP9 was the
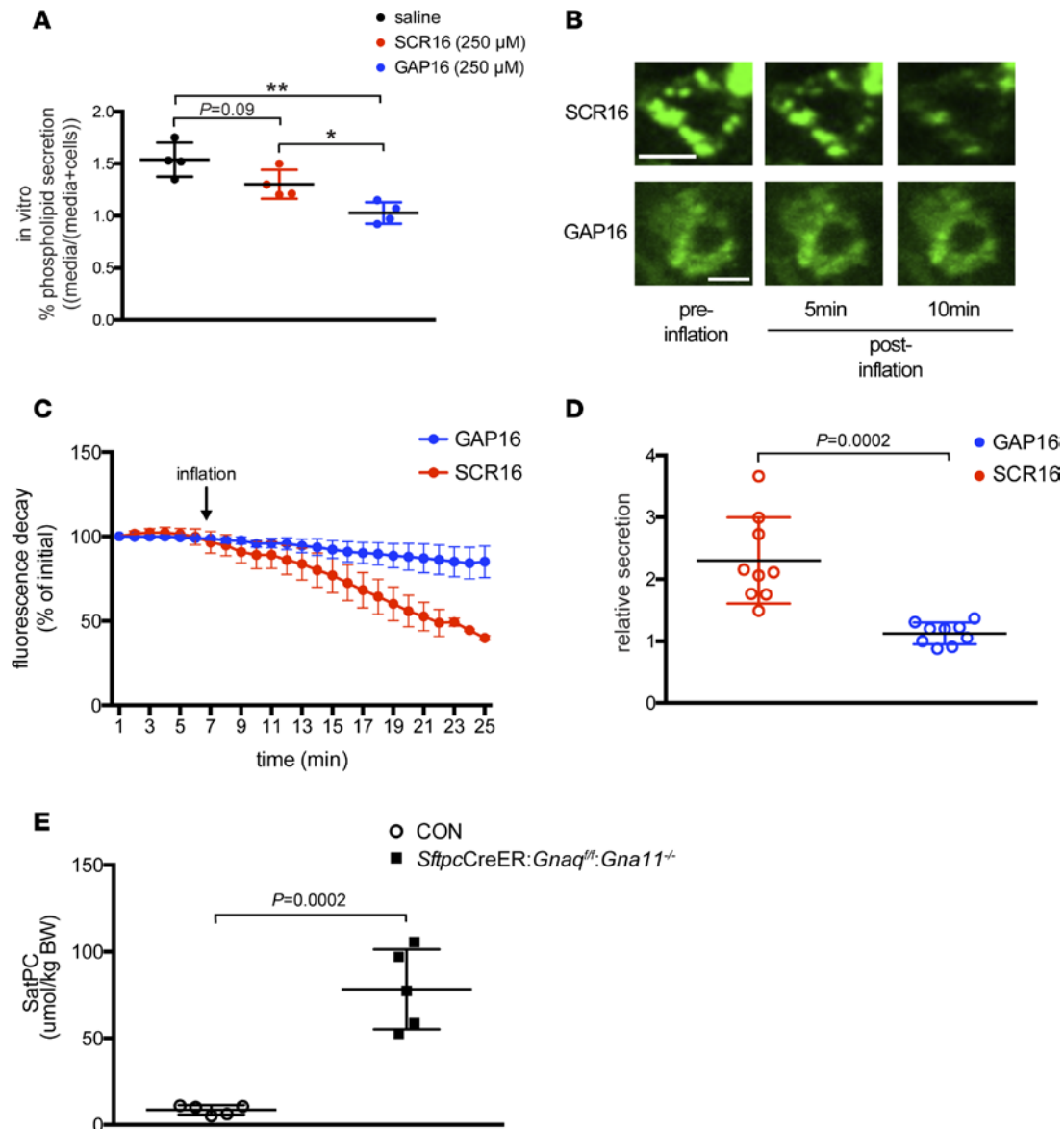
Figure 6. GAP16-induced suppression of surfactant phospholipid secretion and alveolar pool sizes in vivo. (**A**) Basal phospholipid secretion assays in GAP16-treated primary rat AT2 epithelial cells. (**B**–**D**) In vivo secretion assays. Representative in vivo fluorescent images (**B**) of lysotracker green–loaded AT2 cells in intact WT mouse alveoli injected with SCR16 or GAP16 peptide (100 μM). Images represent preinflation and 5 and 10 minutes after 30-second hyperinflation. Scale bar: 5 μm for all images. (**C**) Traces of lysotracker fluorescence as a function of time, before and after hyperinflation. (**D**) Quantitated data from in vivo secretion assays, as performed in **C**. Data represent n = 3 lungs per group, a total of 9 type AT2 cells analyzed per group. (**E**) SatPC levels in bronchoalveolar lavage fluid from 4-week-old *SftpcCreER:Gnaq^{f/f}:Gna11^{-/-}* mice. Mice were placed on tamoxifen chow for 4 weeks prior to harvest (n = 5 mice per group, n = 1 experiment). CON, littermate controls. Data are expressed as mean ± SD. *P < 0.05, **P < 0.01 (1-way ANOVA for **C**–**E**).

minimal active peptide, and GAP10 and GAP12 were the most potent peptides (all peptide sequences and corresponding EC$_{50}$ data are listed in Supplemental Table 1 and 2, respectively). hGPR116 was consistently less sensitive to peptide activation. GPR116-activating peptides failed to induce calcium responses in parental HEK cells, while GAP16 peptides corresponding to mouse and human ectodomain sequences elicited similar responses in HEK cells stably expressing hGPR116 (Supplemental Figure 3, C and D).

GAP16 suppresses basal surfactant phospholipid secretion and alveolar pool sizes in vivo. To determine if GAP16 was sufficient to suppress surfactant secretion from AT2 cells, surfactant phospholipid secretion assays were performed in primary rat AT2 cells due to the robust responsiveness of these cells to secretagogues as compared with primary mouse AT2 cells. GAP16 stimulation inhibited basal phospholipid secretion (Figure 6A). To determine if GAP16 stimulation of GPR116 influenced surfactant secretion in mice in vivo, we
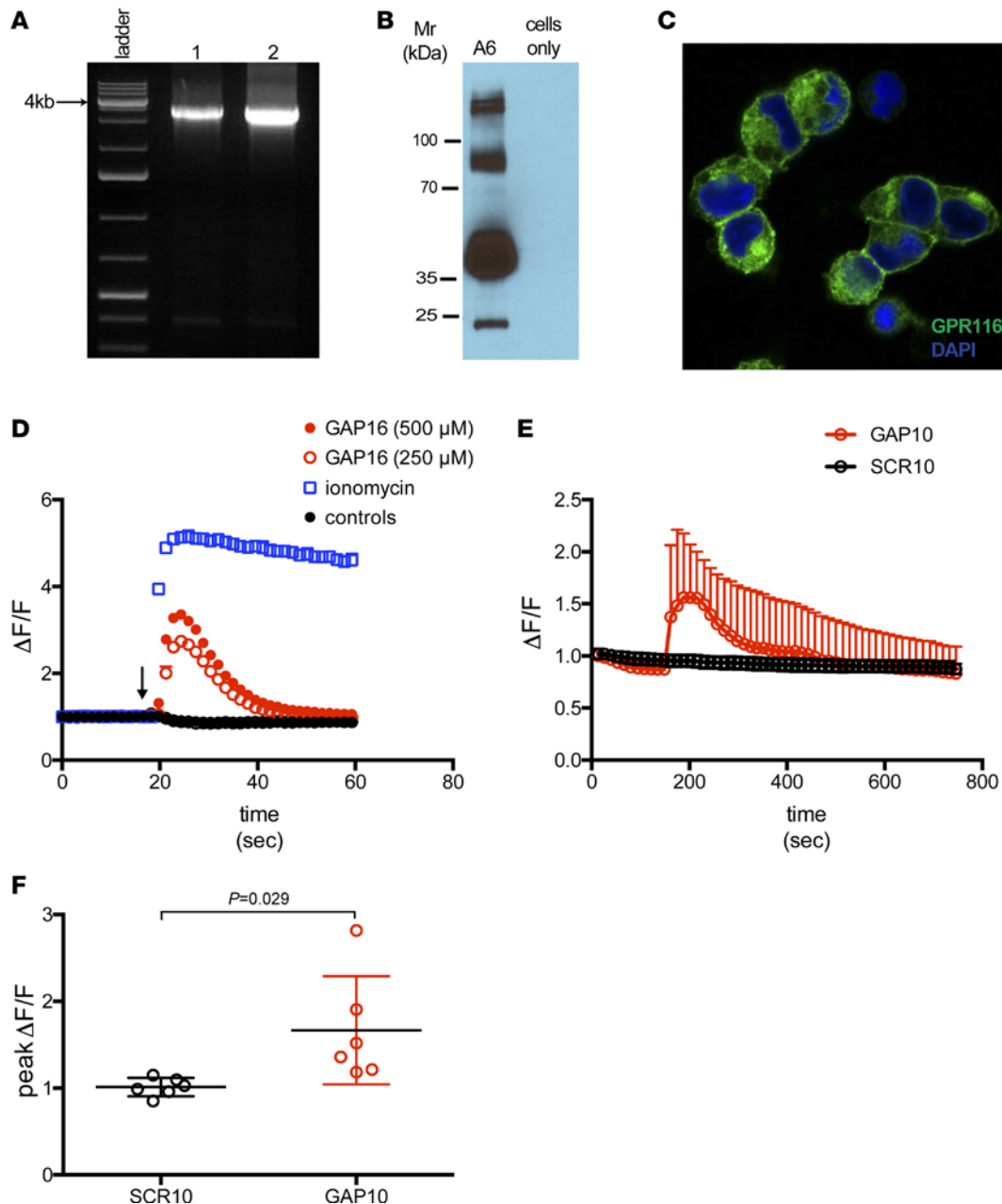
Figure 7. Expression and activation of human GPR116 in transfected and primary human alveolar epithelial cells. (**A**) RT-PCR of full-length GPR116 mRNA from two primary human lung tissue samples. (**B**) Western analysis of HEK293 cell lysates stably transfected with V5-tagged human GPR116 cDNA (A6) versus nontransfected cells. (**C**) Confocal image of A6 cells stained with anti-V5 antibody (green) and DAPI (blue). Original magnification, ×60. (**D**) Representative traces of FLIPR-based calcium mobilization assay in the A6 hGPR116-V5 cell line. Cells were stimulated with 250 μM or 500 μM GAP16 (top and bottom red trace, respectively), 250 μM or 500 μM SCR control, or 1 μM ionomycin. The arrow indicates time of compound addition. (**E** and **F**) Calcium transient tracings (**E**) and quantitation of Fluo-4–based imaging–based calcium transient assays (**F**) in primary human AT2 epithelial cells. Cells were stimulated with 500 μM GAP10 or SCR10 peptide as indicated. Data are expressed as mean ± SD (1-way ANOVA for **C**–**E**).

employed real-time confocal-imaging secretion assays in live mice using a perfused in situ model (44). Surfactant secretion was induced by a single hyperinflation, as shown in representative images (Figure 6B). Surfactant secretion was markedly increased 5 and 10 minutes after inflation in mice treated with the scrambled control peptide (SCR). In contrast, fluorescence was largely maintained at preinflation levels in GAP16-injected animals, indicating suppression of surfactant secretion from AT2 cells (Figure 6, C and D).

We sought to determine if GNAQ/GNA11 signaling in AT2 cells is required for surfactant homeostasis in vivo. Since both *Gnaq* and *Gna11* are expressed in mouse AT2 cells (45) and demonstrate functional redundancy in several tissues (46, 47), we employed a strategy to delete *Gnaq* and *Gna11* in mouse AT2 cells using the
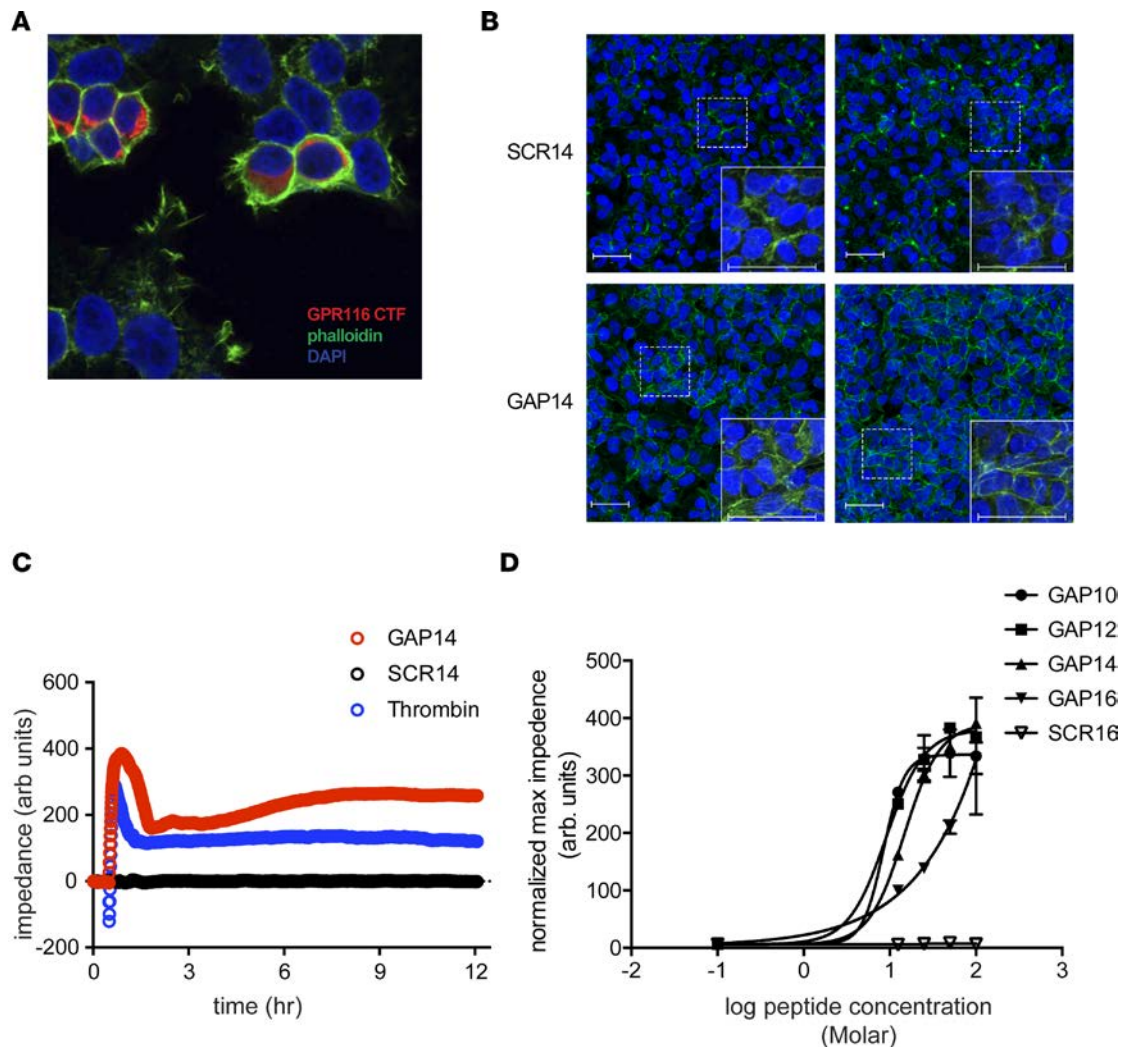
Figure 8. GPR116 regulates cortical actin assembly and barrier function. (A) Increased cortical F-actin staining in HEK293 cells transiently transfected with GPR116 CTF/mCherry for 48 hours compared with mCherry-negative control cells (red = GPR116 CTF/mCherry, green = phalloidin, blue = DAPI). Original magnification, ×60. **(B)** Increased cortical actin staining in GAP14-treated HEK293 cells stably expressing GPR116 (cell line 3C) compared with cells treated with SCR14 peptide (green = phalloidin, blue = DAPI). Scale bar: 50 μm for large images and insets; insets are magnified images of regions denoted by dashed boxes. **(C)** Representative cell impedance traces as a function of time for HEK cells stably expressing mGPR116 treated with mGAP14, scrambled peptide (SCR14), or thrombin as a positive control for Gq signaling. **(D)** Cell impedance measurements in HEK cells stably expressing mGPR116 following stimulation with activating peptides (GAP10, -12, -14, and -16) compared with cells treated with SCR16. Data are expressed as mean ± SD (1-way ANOVA for **C** and **D**).

*Sftpc*CreER driver. *Sftpc*CreER-specific deletion of *Gnaq* on a *Gna11*-deficient background resulted in a 9-fold increase in alveolar surfactant pools (Figure 6E), consistent with the pulmonary phenotype in *Shh*Cre:*Gpr116*^{-/-} and *Sftpc*CreER:*Gpr116*[f/f] animals (Figure 1A). Collectively, these data demonstrate that peptide-induced activation of GPR116 rapidly and potently suppresses pulmonary surfactant secretion ex vivo and in vivo and that the GNAQ/GNA11 signaling pathway downstream of GPR116 in AT2 cells controls surfactant homeostasis.

Expression and activation of hGPR116 in transfected and primary human AT2 cells. To assess the role of GPR116 in human cells, we demonstrated expression of *Gpr116* mRNA in human lung samples, cloned full-length h*Gpr116* cDNA, and generated cell lines stably expressing hGPR116 (Figure 7, A–C; see complete unedited blots in the supplemental material). GAP16 peptide induced rapid Ca^{2+} mobilization in cells stably expressing hGPR116 (Figure 7D), demonstrating conservation of G protein signaling by mGPR116 and hGPR116. To determine if GPR116-activating peptides activate G$_{q/11}$ signaling downstream of endogenous hGPR116, Ca^{2+} mobilization assays were performed in primary human AT2 cells. Culture conditions that maintained AT2 cell differentiation were utilized for these experiments, as the cells contained numerous Lysotracker-positive lamellar bodies and expressed *Gpr116* and AT2 cell–specific markers *Sftpc* and *Abca3* (Supplemental Figure 4). As shown in Figure 7, E and F, GAP10 induced intracellular Ca^{2+} transients in primary human AT2 cells

(Supplemental Videos 3 and 4). These data demonstrate that the proximal signaling events downstream of GPR116 activation are conserved in mouse and human AT2 cells.

GPR116 activation induces cortical F-actin assembly. In vitro and in vivo studies implicate cytoskeletal remodeling processes in the regulation of surfactant secretion and uptake (18, 48–56). We therefore sought to determine if constitutively active GPR116 CTF caused F-actin organization in HEK cells. As shown in Figure 8A, GPR116 CTF caused cortical F-actin assembly. Likewise, activation of full-length GPR116 by GAP14 increased cortical F-actin assembly (Figure 8B).

With cortical F-actin rearrangement serving as an important readout correlated with AT2 cell function, we evaluated the modulation of cellular impedance following activation of GPR116. GAP14 caused a rapid and transient increase in impedance consistent with $G_{q/11}$ coupling (Figure 8C). Consistent with the increased cortical F-actin response, we observed a concentration-dependent increase in maximal impedance after addition of GPR116-activating peptides (Figure 8D), which supports the concept that GPR116 controls surfactant secretion and uptake via modulation of actin dynamics in AT2 cells. Collectively, these data implicate GPR116-driven, $G_{q/11}$-dependent actin remodeling in the regulation of surfactant homeostasis.

Discussion

While previous data implicated GPR116 pulmonary surfactant homeostasis and lung function (33–37), the downstream signaling pathways and mechanisms of action of GPR116 in AT2 cells were unclear. Present studies demonstrate that AT2 cell–specific deletion of *Gpr116* causes alveolar surfactant overload associated with altered surfactant secretion and uptake in AT2 cells. We demonstrate that the ectodomain of GPR116 CTF activates $G_{q/11}$-dependent signaling and that peptides corresponding to the CTF ectodomain cause $G_{q/11}$-dependent signaling. Activating CTF peptides cause calcium transients in primary mouse and human AT2 cells and suppress surfactant secretion from primary rat AT2 cells in vitro and in vivo. AT2 cell–specific deletion of *Gnaq* and *Gna11* causes similar surfactant accumulation in vivo, consistent with findings in *Gpr116*$^{-/-}$ mice. Activation of GPR116 caused actin cytoskeletal rearrangements and increased epithelial impedance downstream of GPR116. Collectively, these data implicate a GPR116-driven, $G_{q/11}$-dependent actin remodeling pathway in the regulation of AT2 cell surfactant homeostasis.

While GPR116 is an orphan receptor, present data are consistent with a model in which full-length GPR116 is held in an inactive state in the absence of ligand binding to the NTF (Figure 9). Subsequent ligand binding to the NTF fragment, perhaps present in the alveolar lumen, causes a conformational change or complete disengagement of the NTF from the CTF, permitting interaction of the activating CTF ectodomain with the 7TM domains, resulting in receptor activation, $G_{q/11}$ coupling, actin rearrangement, and decreased surfactant secretion/increased surfactant uptake. Hirose et al. postulated that surfactant protein D (SFTPD) is a ligand for GPR116 based on coimmunoprecipitation of SFTPD and GPR116 proteins in a heterologous overexpression system (57). Data demonstrating increased pulmonary surfactant pools in *Sftpd*$^{-/-}$ and *Gpr116*$^{-/-}$ mice, albeit at differing degrees of severity, and the abundance of SFTPD protein in the alveolar lumen support this concept. However, transgenic mice that overexpress SFTPD in the distal lung do not have decreased alveolar surfactant pools, nor do they exhibit signs of respiratory distress (58), as would be predicted if SFTPD activated GPR116 based on data presented herein. We propose an alternative model supported by present data whereby GPR116 activity is modulated in vivo via mechanical stretching of AT2 cells caused by perpetual expansion and compression of the alveoli during the ventilatory cycle. Findings that alveolar surfactant phospholipid concentrations in the lungs of fetal *Gpr116*$^{-/-}$ mice at E18.5 are normal (33) and the rapid increase in pool sizes after birth are consistent with activation of the receptor immediately following the transition to air breathing. In further support of a stretch-induced activation model, GPR126 and GPR114, both AdGPCR family members, are activated by sheer stress (28, 59). The findings that expression of full-length GPR116 is not sufficient to activate $G_{q/11}$-dependent responses and that GPR116 is activated by GAP peptides in primary AT2 cells and in intact mouse lungs suggest that a proportion of the GPR116 pool on AT2 cells represents the full-length, inactive receptor. Mass spectrometry–based proteomic analyses of lavage fluid from healthy control and asthmatic patients identified GPR116 peptides that map to the NTF (60). These data suggest that the GPR116 pathway, with demonstrated importance in mouse alveolar homeostasis, is operative in the human lung and are consistent with removal and/or shedding of the NTF from the CTF upon ligand binding and/or AT2 cell stretch. While current data may support a model by which ventilation regulates alveolar surfactant concentrations, identification of GPR116 ligands or the mode by which GR116 is activated in the alveolar lumen requires further investigation.
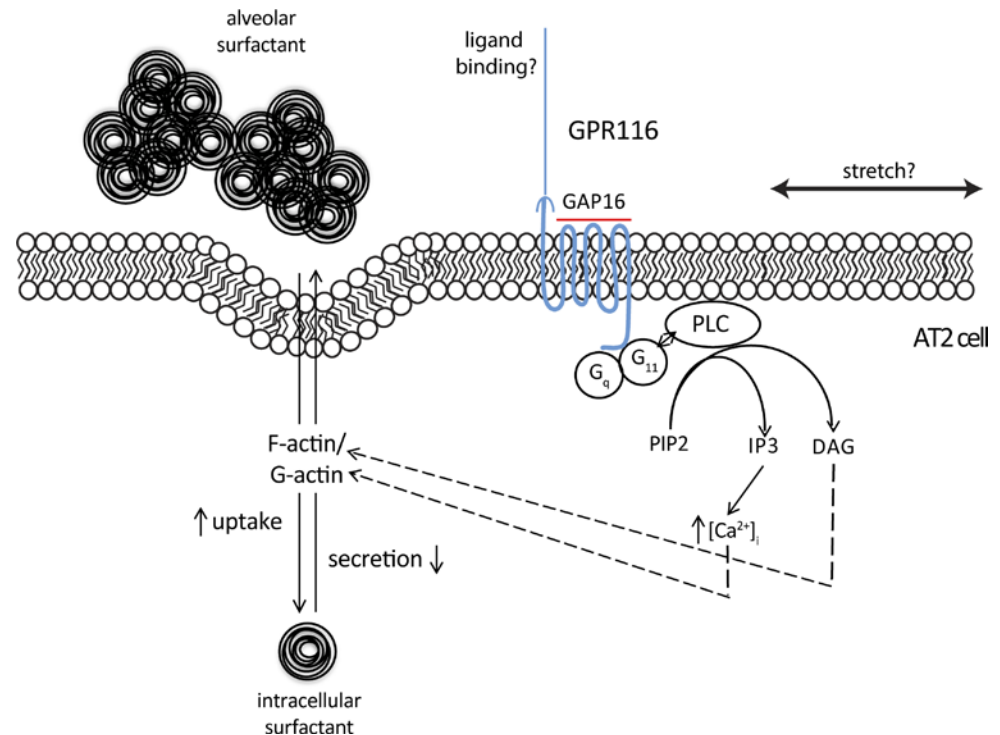
Figure 9. Model of GPR116-mediated modulation of surfactant homeostasis in alveolar type II cells. Present data support a model in which full-length GPR116 is held in an inactive state in the absence of ligand binding to the NTF. Subsequent ligand binding to the NTF fragment, perhaps present in the alveolar lumen, or cell stretch induced by the ventilator cycle induces a conformational change, or complete disengagement of the NTF from the CTF, that permits interaction of the activating CTF ectodomain with the 7TM domains, resulting in receptor activation, $G_{q/11}$ coupling, actin rearrangement, and decreased surfactant secretion/increased surfactant uptake. Activating peptides, such as GAP16, bypass the inhibitory effect of the NTF, resulting in receptor activation.

Our data demonstrating an inhibitory role of GPR116-induced, $G_{q/11}$-dependent calcium transients on surfactant secretion, coupled with recapitulation of the surfactant overload phenotype in *Gnaq:Gna11*-deficient mice, appear paradoxical to the well-described correlation between intracellular calcium concentration and surfactant secretion in isolated AT2 cells. ATP activation of P2RY2 potently stimulates surfactant secretion in isolated AT2 cells in a $G_{q/11}$- and Ca^{2+}-dependent pathway (1). The findings that *P2ry2*^{-/-} mice have normal baseline surfactant levels and deletion of *P2ry2* in *Gpr116*^{-/-} mice does not influence surfactant accumulation indicate that this $G_{q/11}$-coupled receptor is dispensable for surfactant homeostasis in vivo. Recent data demonstrate increased pulmonary inflammation, including foamy macrophages, and alveolar simplification in mice lacking *Gnaq* and *Gna11* in AT2 cells (61), while AT2 cell–specific deletion of *Gna12* and *Gna13* showed no overt pulmonary phenotype. Present data demonstrating rapid and robust accumulation of surfactant in *Sftpc*CreER:*Gnaq:Gna11*-deficient animals are consistent with observations in *Gpr116*^{-/-} mice, suggesting that disrupted surfactant homeostasis in AT2 cells is the primary driver of alveolar remodeling and inflammation in mice lacking $G_{q/11}$ signaling. Current data from primary cells suggest that transient calcium peaks following receptor-mediated activation, as seen following GPR116 activation, may not be the most relevant trigger for exocytosis in isolated AT2 cells (62). Rather, lamellar body exocytosis is dependent upon sustained increases in cytoplasmic calcium, with an additional role for extracellular calcium entry caused by lamellar body fusion to the plasma membrane (63). Differential calcium responses with respect to surfactant secretion may also result from compartmentalization of calcium signals and/or differential effects on local calcium levels within AT2 cells. Detailed mechanisms of calcium signaling in AT2 cells downstream of GPR116 activation remain to be determined.

The GPR116 CTF domain and synthetic CTF peptides activated GPR116, causing a pronounced increase in cortical F-actin assembly and cell impedance in HEK cells. Actin cytoskeletal remodeling was implicated in the regulation of surfactant secretion and uptake in vitro and in vivo; however, the precise role of actin in surfactant homeostasis remains unclear, as cell and animal studies report both suppression

and augmentation of secretion following actin cytoskeletal disruption (18, 48–52). Tang et al. reported that endogenous hGPR116 regulates F-actin stress fiber formation and cell motility in transformed MDA-MB-231 breast cancer cells in a $G_q/_{11}$- and Rho-dependent manner (64). As AT2 cells are nonmotile, secretory epithelial cells, F-actin modulation downstream of GPR116 in AT2 cells is likely to have distinct functions in lung epithelial cells. The molecular pathway(s) integrating actin cytoskeletal rearrangement and surfactant secretion/uptake downstream of GPR116 and $G_{q/11}$ activation in AT2 cells represents an important area of future study.

In summary, the identification of GPR116-activating peptides that regulate surfactant secretion and uptake provides therapeutic approaches to positively or negatively regulate endogenous surfactant concentrations for patients with pulmonary surfactant–related disorders. Our data demonstrating suppression of alveolar surfactant levels following administration of GPR116-activating peptides provides proof of concept that GPR116 is a plausible target for treatment of pulmonary diseases associated with surfactant dysfunction. Suppression of surfactant secretion or enhancement of uptake through inhibition of GPR116 may be useful in treating diseases caused by surfactant accumulation, including pulmonary alveolar proteinosis. We speculate that inhibition of GPR116 may be useful in the treatment of lung diseases caused by loss of surfactant, as occurs in acute respiratory distress syndromes.

Methods

Animals. *Gpr116*$^{-/-}$ and *Gpr116*$^{f/f}$ mice have been described previously (33). *Shh*Cre (stock 005622), *Tie2*Cre mice (stock 008863), *P2ry2*$^{-/-}$ mice (stock 009132), and WT C57BL/6J mice (stock 000664) were purchased from Jax labs. *SftpcCre*ER mice were a gift of Brigid Hogan (Duke University, Durham, North Carolina, USA). *Gnaq*$^{f/f}$:*Gna11*$^{-/-}$ mice have been previously described (47). Tamoxifen chow containing 400 mg/kg (Envigo) was given ad libitum to 4-week-old *SftpcCre*ER:*Gpr116*$^{f/f}$ mice and 8-week-old *SftpcCre*ER:*Gnaq*$^{f/f}$:*Gna11*$^{-/-}$ mice to induce deletion of *Gpr116* and *Gnaq* in the context of *Gna11*$^{-/-}$, respectively, in AT2 cells. Mice used in this study were between the ages of 4 and 12 weeks and were appropriately age matched (within 1 week) and gender matched. Mice were on a mixed background consisting of C57BL/J and BALB/c; littermates were used as controls for all experiments to account for any possible strain-dependent effects. Because of the markedly different phenotypes of the WT *Gpr116*-deficient animals, randomization and blinding were not used for animal experiments. No mice were excluded. Sample sizes of 3–4 mice per group, per experiment, were chosen, based on our previously published data using the same experimental readouts (33).

Isolation of primary AT2 cells (mouse, rat, and human). Mouse AT2 cells were isolated via a dispase-based digestion method as previously described (43). Rat type AT2 cells were isolated via an elastase-based digestion method, followed by panning with rat IgG-coated plates, and cultured on 12-well tissue culture plastic as previously described for 2 days prior to stimulation (65). Primary human AT2 cells were isolated from human lungs from deidentified organ donors whose lungs were not suitable for transplantation. The lung was perfused, lavaged, and digested with elastase as described previously (66). The lung was minced, and the cells were partially purified by centrifugation on a discontinuous density gradient made of Optiprep (Accurate Chemical Scientific Corp.) with densities of 1.080 and 1.040. The AT2 cells were then isolated either by nonadherence to IgG-coated petri dishes or positive selection with MACS MicroBeads human CD326 (EpCAM, clone HEA-125) (Miltenyi Biotech) (67). The magnetic bead separation produces a slightly higher purity but worse plating efficiency than the IgG method. Both methods result in similar purity after plating in culture. The isolated cells were frozen down in 90% fetal calf serum and 10% DMSO. For calcium imaging experiments, cells were thawed and cultured in BEGM, 10% charcoal-stripped FBS, and recombinant human KGF (10 ng/ml, Peprotech) on top of a thin substrate of 70% Cultrex (Trevigen)/30% rat tail collagen (Advanced Biomatrix) coated onto 35-mM dishes with a coverslip bottom (MatTek) to maintain a differentiated phenotype. Human AT2 cells were cultured for 7 days prior to experimentation.

Calcium imaging assays. Primary mouse and human AT2 cells were cultured in BEGM, 10% charcoal-stripped FBS, and recombinant human KGF (10 ng/ml, Peprotech) on top of a thin substrate of 70% Cultrex (Trevigen)/30% rat tail collagen (Advanced Biomatrix) coated onto 35-mM dishes with a coverslip bottom (MatTek) to maintain a differentiated phenotype. Mouse cells were cultured for 5 days after isolation prior to experimentation. Human AT2 cells were cultured for 7 days after thawing prior to experimentation. On the day of experimentation, media were replaced with 1 ml Krebs-Ringer's buffer plus 1.8 mM calcium chloride and incubated for 30 minutes at 37°C to equilibrate. Cells were washed once with

Krebs-Ringer's buffer plus 1.8 mM calcium chloride and loaded with Fluo-4 AM (1 μg/μl; ThermoFisher) plus 10 μl 0.2% pluronic acid for 30 minutes at 37°C. Cells were washed 4 times with 1 ml with Krebs-Ringer's plus calcium buffer, leaving the last 1 ml on cells to image. Time-lapse imaging was performed on an Olympus IX51 (mouse AT2) or Nikon Spectra X (human AT2) wide-field fluorescent microscope.

Imaging alveolar secretion in vivo by confocal microscopy. Mice were anesthetized and exsanguinated. Hearts and lungs were then removed en block, placed on a Petri dish, and covered with moistened plastic wrap. The lung preparation was then placed on a microscope stage and pump perfused with autologous blood (14 ml/min) at 37°C. The pulmonary artery, left atrial, and airway pressures were held constant at 10, 3, and 5 cm H_2O, respectively. The lung surface was visualized under bright-field illumination. A single alveolus was micropunctured and instilled with mineral oil mixed with Sudan Black as a spatial marker. Then, a nearby alveolus was micropunctured and instilled with lysotracker green DND-26 (75 nM; ThermoFisher) plus either GAP16 (100 μM) or SCR16 (100 μM) for 30 minutes. Following instillation, the lung surface was illuminated with a 488-nm laser. Confocal images of the resulting lysotracker green fluorescence were captured using a Zeiss 710 imaging system. Images were captured at 1-minute intervals. Following a 5- to 7-minute baseline recording, lungs were inflated to 15 cm H_2O for 30 seconds. After inflation, confocal images were again obtained at 1-minute intervals for a total of 10 minutes. Resultant images were analyzed using ImageJ (NIH) software.

GPR116 cDNA constructs. Full-length mGPR116 and hGPR116 were tagged at the C-terminus with FLAG or V5 tag sequence using PCR-based techniques. mGPR116 CTF constructs consisted of the following: a bovine prolactin signal sequence (to direct the chimeric proteins to the cell surface, as previously described, ref. 68), a 1X FLAG tag, and a mGPR116 sequence immediately downstream of the GPS cleavage site. Alanine point mutant constructs were generated using PCR-based techniques with mGPR116 CTF cDNA as a template. All cDNAs were inserted into CMV-driven, pcDNA3-based vectors (Invitrogen) for expression in mammalian cells.

Generation of Gpr116 stable cell lines. HEK293 cells (ATCC) were grown in DMEM/HAMs F12 medium supplemented with 10% FCS and 1% penicillin/streptomycin. For selection and maintenance of stably transfected cells, G418 (400 μg/ml) was added to the culture medium. hGpr116 (AB018301.2) and mGPR116 (NM_001081178.1) cDNAs were cloned into pcDNA3.1-Topo and pcDNA3.1-Topo V5 His plasmids and transfected into HEK293 cells for transient expression assays or linearized with PvuI for transfection into HEK293 cells for generation of stable clones. For stable transfection, cells were seeded in a 4-cm Petri dish to reach 80% confluence the next day. Transfection was carried out using 4 μl Lipofectamine 2000 reagent (Invitrogen, catalog 11668) and 2 μg linearized plasmid DNA, according to the manufacturer's instructions. After overnight incubation, cells were split and G418 selection was initiated. Cell clones were collected by mechanical dislocation using a standard pipettor and transferred to 24-well plates for further expansion. Stable clones selected for downstream assays were clone 3C for mGPR116 (untagged) and clone A6 for hGPR116 (C terminal V5 tagged).

Expression of the GPR116-V5 fusion protein in stably transfected cells, and GPR116 CTF in transiently transfected cells, was analyzed by immunocytochemistry. Briefly, cells were plated in 8-chamber slides (Ibidi, catalog 161107), washed the following day with PBS, fixed and permeabilized for 20 minutes at 4°C, blocked for 20 minutes at room temperature, and stained using an anti-V5 antibody (2 hours, room temperature, 1:500; Invitrogen, catalog R96025) or anti-FLAG antibody (overnight, 4°C, 1:100; Sigma-Aldrich, F1365) followed by an anti-mouse secondary antibody (V5: 1 hour, room temperature, 1:500; Invitrogen, catalog A21200; FLAG: 2 hours, room temperature, 1:200; Invitrogen, A11004) according to the manufacturer's instructions. Nuclei were stained for 3 minutes with Hoechst (Invitrogen, catalog H-3570). Cells were then analyzed by confocal microscopy on a Zeiss LSM700 inverted microscope for GPR116-V5 cells and a Nikon AIR LUN-V inverted microscope for mGPR116 CTF.

Calcium transient assays. HEK293 cells were seeded in 384-well plates (Greiner, 781946) at 15,000 cells/well or in poly-D-lysine–coated 96-well plates at 50,000 cells/well. Medium was removed the following day, and cells were loaded for 2 hours at 37°C, 5% CO_2, with 20 μl calcium 6 loading buffer (Molecular Devices, catalog R8191): 1X HBSS (Gibco, catalog 14065.049) containing 20 mM HEPES (Gibco, catalog 15630) and 2.5 mM probenecid (Sigma-Aldrich, catalog P8761). Plates were then transferred to a FDSS7000 fluorescence plate reader (HAMAMATSU) for 384-well plate assays or a Flexstation 3 fluorescence plate reader (Molecular Devices) for 96-well plate assays, and Ca^{2+} responses were measured in real time using a CCD camera with excitation = 480 nm/emission = 540 nm. Prior to stimulation, baseline measurements were

recorded over 5 seconds (Fmin). For stimulation, 20 μl of test compounds prepared twice in HBSS containing 20 mM HEPES were dispensed. Fluorescence was read over 1 to 1.5 minutes. Maximum fluorescence (Fmax) was determined and normalized to baseline. Data are reported as ΔF/F = (Fmax – Fmin)/Fmin.

GAP-activating peptide synthesis. All peptides used in this study were synthesized by Mimotopes and Peptides and Elephants GmbH. Peptides were dissolved as stock solution in either DMSO or dH_2O at 50 mM for all experiments except the GAP9-16 truncation experiments (10 mM stocks). Amino acid sequences for all peptides are listed in Supplemental Table 1.

Cell impedance measurements by electric cell–substrate impedance sensing. Impedance of cell monolayers was monitored using electric cell–substrate impedance sensing (ECIS) instruments (Applied BioPhysics). Experiments were conducted at 37°C and 5% CO_2 in a humidified incubator. Cells were seeded in 8-well plates with electrodes embedded at the bottom of each well (ECIS 8W 10E or 10E+). Wells were pretreated with 10 mM poly-D-lysine (Sigma-Aldrich, P8920). Cells were seeded at 10,000 cells/well and grown to confluence over 5 to 6 days. Growth medium was then replaced with 180 μl serum-free medium for 4 hours; during the last 1 hour, baseline resistance was measured prior to treatment. Cells were stimulated with 20 μl of 10x compounds and impedance was measured in real time for 12 hours at a frequency of 4,000 Hz and constant current of 1 microampere at 20-second intervals.

F-actin staining and imaging. Cells were seeded into 8-well chambers (Ibidi, 161107) and grown to confluence. On the day of the assay, cells were starved for 5 hours prior to stimulation with the peptides for 1.5 hours. Monolayers were rinsed with PBS, fixed/permeabilized with 200 μl BD Cytofix/Cytoperm (BD Bioscience, 554722) for 20 minutes at 4°C, washed with 500 μl Wash solution 1x (BD Bioscience, 554723), and blocked overnight at 4°C in blocking solution (5% FCS, 1% BSA, 1x Wash solution, supplemented with 10 mM HEPES, 140 mM NaCl, 5 mM $CaCl_2$). Phalloidin (100 μl at 1:100; Invitrogen, A12379) was added for 1 hour in the dark at room temperature, followed by 100 μl Hoechst at 1:1,000 (Invitrogen, H-3570) for an additional 1 hour. Cells were washed 4 times with Wash buffer, and slides were stored in PBS at 4°C in the dark until imaged. Confocal data sets were sampled on a Zeiss LSM 700 inverted microscope; image acquisition and post-processing were performed with proprietary Zeiss software (Zen 2012). Three random Z-stacks were acquired and analyzed for each experimental condition. Data were confirmed in a second independent experiment.

IP accumulation assays. HEK cells were seeded in 12-well plates at a density of 1.5×10^5 cells per well and transiently transfected with plasmids expressing WT, WT mGPR116-FLAG, CTF-FLAG, or alanine mutants of CTF-FLAG. Twenty-four hours after transfection, media were removed and replaced with serum-free Modified Eagles Medium (MEM; Mediatech) containing 1 μCi/ml of ^{3}H-myo-inositol (Perkin-Elmer Life Sciences). Forty-eight hours after infection, media were removed and replaced with serum-free media supplemented with 20 mM LiCl for 3 hours. For samples to be stimulated with GAPs, the peptides were added at the appropriate concentration when the media were replaced with that supplemented with LiCl. Reactions were stopped by aspirating medium, adding 1 ml of 0.4 M perchloric acid, and cooling undisturbed at 4°C for 5 minutes. 800 μl of supernatant was neutralized with 400 μl of 0.72 M KOH/0.6 M $KHCO_3$ and subjected to centrifugation. 1 ml of supernatant was diluted with 3 ml of distilled H_2O and applied to freshly prepared Dowex columns (AG1-X8; Bio-Rad). Columns were washed two times with distilled H_2O, total IPs were eluted with 4.0 ml of 0.1 M formic acid and 1 M ammonium formate, and eluates containing accumulated IPs were counted in a liquid scintillation counter. 50 μl of neutralized supernatant was counted in a liquid scintillation counter to measure total incorporated ^{3}H-myo-inositol. Data are expressed as accumulated IP over total incorporated ^{3}H-myo-inositol.

SatPC measurements. BALF was collected by intratracheal intubation followed by serial lavaging with 0.9% saline (5×1 ml total, pooled and placed on ice). Lipids were extracted from the lavage by the Bligh and Dyer method (69). SatPC was isolated using the osmium tetroxide-based method of Mason et al. (70) and quantitated by phosphorous measurement. SatPC levels in BALF reported here represent the total BALF, including the BAL cell pellet.

PL secretion assays. ^{3}H-phosphatidylcholine secretion was assessed as previously described for rat AT2 cells (1). AT2 cells were labeled with 1 μCi/ml ^{3}H-choline (Perkin Elmer) for 24 hours before assay 7 days in culture. Cells were washed to remove free label, and secretagogues or inhibitors were added at time 0. Media were removed after 3 hours, and cells were rinsed with 0.5 ml of fresh media. The media samples were combined, and cells were removed by centrifugation (130 *g* for 10 minutes). Lipids were extracted with chloroform/methanol (2:1), and the lipid phases were evaporated to dryness. Lipid disintegrations per

minute (dpm) present in the media and cell samples were determined, and the percentage of phospholipid secretion was calculated as dpm media/(dpm media + dpm cells) × 100%.

Small aggregate surfactant isolation and surfactant uptake assays. Small aggregate (SA) surfactant was isolated as previously described (71). In brief, BAL was performed 5 times with 1 ml 0.9% saline. BALF was centrifuged at 4,000 *g* over a 0.8 M sucrose cushion for 15 minutes. Large aggregate surfactant was collected from the interface, diluted with 15 mM NaCl, and centrifuged again at 40,000 *g* for 15 minutes. The supernatant that was centrifuged at 40,000 *g* that contained SA surfactant was pelleted by centrifugation at 100,000 *g* for 24 hours, and total phospholipids were quantitated by phosphorous assay.

AT2 cells were isolated from control and *Gpr116−/−* mice and cultured as previously reported (33, 43). The rate of SA surfactant uptake by AT2 cells was studied 5 days following AT2 cell isolation. SA containing 15 nmol total phospholipid were labeled by mixing with 4.8 μg *N*-rhodamine dipalmitoylphosphatidylethanolamine (Avanti Polar Lipids). Fluorescently labeled SA were added to the cultured AT2 cells from control and *Gpr116−/−* mice. After a 0.5-, 2-, and 4.5-hour incubation, cells were carefully washed 5 times with PBS and extracted with methanol containing 1 mg/ml dipalmitoylphosphatidylcholine. Fluorescence was measured on a SpectraMax plate reader (Molecular Devices) with excitation = 510 nm/emission = 565 nm.

Western analysis. Total protein concentration of the cell lysates was determined by BCA assay (Pierce), and equal amounts of protein were separated by SDS-PAGE. Proteins were electrophoretically transferred to nitrocellulose membranes and probed with a monoclonal antibody directed against V5 (clone V5-10, Sigma-Aldrich V8012) or FLAG (clone M2, Sigma-Aldrich F1365). Stripping of the antibody complexes was performed using Restore Western blot stripping buffer (Pierce), and blots were reprobed with a monoclonal antibody directed against actin (clone B4, Seven Hills Bioreagents).

Statistics. All data met the assumption of the statistical tests; variances were similar between the groups of statistical comparison. Two-tailed Student's *t* tests and ANOVA were performed for all experiments to determine the significance of differences between groups. A *P* value of less than 0.05 was considered significant. All experiments were replicated at least twice, as indicated in the figure legends, except lipid analysis on *SftpcCreER:Gnaq^{f/f}:Gna11−/−* and littermate control mice, which was performed once on *n* = 5 mice per group. When feasible, investigators were blinded to groups for cell-based studies and experiments were replicated in two separate laboratories (Cincinnati Children's Hospital Medical Center and Novartis), including calcium assays for in vitro peptide activation experiments, F-actin imaging experiments, selected CTF alanine mutagenesis experiments, and cAMP assays following GAP16 stimulation. An individual mouse or an individual well of cells was counted as 1 sample for all statistical analyses.

Study approval. The Institutional Animal Use and Care Committee at Cincinnati Children's Hospital Medical Center approved all animal studies (IACUC2013-0004), which were carried out in accordance with the NIH's *Guide for the Care and Use of Laboratory Animals* (National Academies Press, 2011). Mice were anesthetized and exsanguinated in accordance with protocols approved by the Institutional Animal Care and Use Committee of the University of Tennessee Health Science Center. The Committee for the Protection of Human Subjects at National Jewish Health deemed this research as nonhuman subject research.

Author contributions

JPB and MGL developed the concept. JPB, MGL, and KS designed the experiments, interpreted the data, and wrote the manuscript. KB, AF, JJ, KA, KK, KP, and SV conducted the experimental work, with help from APN for calcium imaging studies and from WEP for the IP assays. RJM isolated and provided the primary human AT2 cells for calcium imaging studies. SO provided *Gnaq^{f/f}:Gna11−/−* mice. JAW assisted in editing of the manuscript and interpretation of the data.

Acknowledgments

Address correspondence to: James P. Bridges, 3333 Burnet Avenue, ML7029, Cincinnati, Ohio 45229, USA. Phone: 513.636.0337; E-mail: james.bridges@cchmc.org.

1. Rice WR, Singleton FM. P2-purinoceptors regulate surfactant secretion from rat isolated alveolar type II cells. *Br J Pharmacol*. 1986;89(3):485–491.

2. Gilfillan AM, Rooney SA. Purinoceptor agonists stimulate phosphatidylcholine secretion in primary cultures of adult rat type II pneumocytes. *Biochim Biophys Acta*. 1987;917(1):18–23.

3. Dobbs LG, Mason RJ. Pulmonary alveolar type II cells isolated from rats. Release of phosphatidylcholine in response to beta-adrenergic stimulation. *J Clin Invest*. 1979;63(3):378–387.

4. Mettler NR, Gray ME, Schuffman S, LeQuire VS. beta-Adrenergic induced synthesis and secretion of phosphatidylcholine by isolated pulmonary alveolar type II cells. *Lab Invest*. 1981;45(6):575–586.

5. Brown LA, Longmore WJ. Adrenergic and cholinergic regulation of lung surfactant secretion in the isolated perfused rat lung and in the alveolar type II cell in culture. *J Biol Chem*. 1981;256(1):66–72.

6. Gilfillan AM, Rooney SA. Functional evidence for adenosine A2 receptor regulation of phosphatidylcholine secretion in cultured type II pneumocytes. *J Pharmacol Exp Ther*. 1987;241(3):907–914.

7. Griese M, Gobran LI, Douglas JS, Rooney SA. Adenosine A2-receptor-mediated phosphatidylcholine secretion in type II pneumocytes. *Am J Physiol*. 1991;260(2 Pt 1):L52–L60.

8. Wirtz HR, Dobbs LG. Calcium mobilization and exocytosis after one mechanical stretch of lung epithelial cells. *Science*. 1990;250(4985):1266–1269.

9. Ikegami M, Whitsett JA, Jobe A, Ross G, Fisher J, Korfhagen T. Surfactant metabolism in SP-D gene-targeted mice. *Am J Physiol Lung Cell Mol Physiol*. 2000;279(3):L468–L476.

10. Rebello CM, Jobe AH, Eisele JW, Ikegami M. Alveolar and tissue surfactant pool sizes in humans. *Am J Respir Crit Care Med*. 1996;154(3 Pt 1):625–628.

11. Jobe A, Ikegami M, Jacobs H. Changes in the amount of lung and airway phosphatidylcholine in 0.5-12.5-day-old rabbits. *Biochim Biophys Acta*. 1981;664(1):182–187.

12. Ikegami M. Surfactant catabolism. *Respirology*. 2006;11 Suppl:S24–S27.

13. Rice WR, Hull WM, Dion CA, Hollinger BA, Whitsett JA. Activation of cAMP dependent protein kinase during surfactant release from type II pneumocytes. *Exp Lung Res*. 1985;9(1-2):135–149.

14. Sano K, Voelker DR, Mason RJ. Involvement of protein kinase C in pulmonary surfactant secretion from alveolar type II cells. *J Biol Chem*. 1985;260(23):12725–12729.

15. Voyno-Yasenetskaya TA, Dobbs LG, Williams MC. Regulation of ATP-dependent surfactant secretion and activation of second-messenger systems in alveolar type II cells. *Am J Physiol*. 1991;261(4 Suppl):105–109.

16. Liu L. Inhibition of lung surfactant secretion by KN-62, a specific inhibitor of the calcium- and calmodulin-dependent protein kinase II. *Biochem Mol Biol Int*. 1998;45(4):823–830.

17. Nicholas TE, Barr HA. The release of surfactant in rat lung by brief periods of hyperventilation. *Respir Physiol*. 1983;52(1):69–83.

18. Islam MN, Gusarova GA, Monma E, Das SR, Bhattacharya J. F-actin scaffold stabilizes lamellar bodies during surfactant secretion. *Am J Physiol Lung Cell Mol Physiol*. 2014;306(1):L50–L57.

19. Ashino Y, Ying X, Dobbs LG, Bhattacharya J. [Ca(2+)](i) oscillations regulate type II cell exocytosis in the pulmonary alveolus. *Am J Physiol Lung Cell Mol Physiol*. 2000;279(1):L5–13.

20. Nicholas TE, Power JH, Barr HA. The pulmonary consequences of a deep breath. *Respir Physiol*. 1982;49(3):315–324.

21. Yang D, et al. The A2B adenosine receptor protects against inflammation and excessive vascular adhesion. *J Clin Invest*. 2006;116(7):1913–1923.

22. Homolya L, Watt WC, Lazarowski ER, Koller BH, Boucher RC. Nucleotide-regulated calcium signaling in lung fibroblasts and epithelial cells from normal and P2Y(2) receptor (-/-) mice. *J Biol Chem*. 1999;274(37):26454–26460.

23. Chruscinski AJ, Rohrer DK, Schauble E, Desai KH, Bernstein D, Kobilka BK. Targeted disruption of the beta2 adrenergic receptor gene. *J Biol Chem*. 1999;274(24):16694–16700.

24. Fukuzawa T, Hirose S. Multiple processing of Ig-Hepta/GPR116, a G protein-coupled receptor with immunoglobulin (Ig)-like repeats, and generation of EGF2-like fragment. *J Biochem*. 2006;140(3):445–452.

25. Langenhan T, Aust G, Hamann J. Sticky signaling–adhesion class G protein-coupled receptors take the stage. *Sci Signal*. 2013;6(276):re3.

26. Iguchi T, Sakata K, Yoshizaki K, Tago K, Mizuno N, Itoh H. Orphan G protein-coupled receptor GPR56 regulates neural progenitor cell migration via a G alpha 12/13 and Rho pathway. *J Biol Chem*. 2008;283(21):14469–14478.

27. Demberg LM, Rothemund S, Schöneberg T, Liebscher I. Identification of the tethered peptide agonist of the adhesion G protein-coupled receptor GPR64/ADGRG2. *Biochem Biophys Res Commun*. 2015;464(3):743–747.

28. Wilde C, et al. The constitutive activity of the adhesion GPCR GPR114/ADGRG5 is mediated by its tethered agonist. *FASEB J*. 2016;30(2):666–673.

29. Bohnekamp J, Schöneberg T. Cell adhesion receptor GPR133 couples to Gs protein. *J Biol Chem*. 2011;286(49):41912–41916.

30. Mogha A, et al. Gpr126 functions in Schwann cells to control differentiation and myelination via G-protein activation. *J Neurosci*. 2013;33(46):17976–17985.

31. Liebscher I, et al. A tethered agonist within the ectodomain activates the adhesion G protein-coupled receptors GPR126 and GPR133. *Cell Rep*. 2014;9(6):2018–2026.

32. Stoveken HM, Hajduczok AG, Xu L, Tall GG. Adhesion G protein-coupled receptors are activated by exposure of a cryptic tethered agonist. *Proc Natl Acad Sci USA*. 2015;112(19):6194–6199.

33. Bridges JP, et al. Orphan G protein-coupled receptor GPR116 regulates pulmonary surfactant pool size. *Am J Respir Cell Mol Biol*. 2013;49(3):348–357.

34. Abe J, Suzuki H, Notoya M, Yamamoto T, Hirose S. Ig-hepta, a novel member of the G protein-coupled hepta-helical receptor

(GPCR) family that has immunoglobulin-like repeats in a long N-terminal extracellular domain and defines a new subfamily of GPCRs. *J Biol Chem*. 1999;274(28):19957–19964.

35. Ariestanti DM, Ando H, Hirose S, Nakamura N. Targeted disruption of Ig-Hepta/Gpr116 causes emphysema-like symptoms that are associated with alveolar macrophage activation. *J Biol Chem*. 2015;290(17):11032–11040.

36. Yang MY, et al. Essential regulation of lung surfactant homeostasis by the orphan G protein-coupled receptor GPR116. *Cell Rep*. 2013;3(5):1457–1464.

37. Niaudet C, et al. Gpr116 receptor regulates distinctive functions in pneumocytes and vascular endothelium. *PLoS ONE*. 2015;10(9):e0137949.

38. Harfe BD, Scherz PJ, Nissim S, Tian H, McMahon AP, Tabin CJ. Evidence for an expansion-based temporal Shh gradient in specifying vertebrate digit identities. *Cell*. 2004;118(4):517–528.

39. Rock JR, et al. Multiple stromal populations contribute to pulmonary fibrosis without evidence for epithelial to mesenchymal transition. *Proc Natl Acad Sci USA*. 2011;108(52):E1475–E1483.

40. Nishimura A, et al. Structural basis for the specific inhibition of heterotrimeric Gq protein by a small molecule. *Proc Natl Acad Sci USA*. 2010;107(31):13666–13671.

41. Katz A, Wu D, Simon MI. Subunits beta gamma of heterotrimeric G protein activate beta 2 isoform of phospholipase C. *Nature*. 1992;360(6405):686–689.

42. Goel R, Phillips-Mason PJ, Gardner A, Raben DM, Baldassare JJ. Alpha-thrombin-mediated phosphatidylinositol 3-kinase activation through release of Gbetagamma dimers from Galphaq and Galphai2. *J Biol Chem*. 2004;279(8):6701–6710.

43. Bridges JP, Ikegami M, Brilli LL, Chen X, Mason RJ, Shannon JM. LPCAT1 regulates surfactant phospholipid synthesis and is required for transitioning to air breathing in mice. *J Clin Invest*. 2010;120(5):1736–1748.

44. Ichimura H, Parthasarathi K, Lindert J, Bhattacharya J. Lung surfactant secretion by interalveolar Ca2+ signaling. *Am J Physiol Lung Cell Mol Physiol*. 2006;291(4):L596–L601.

45. Ludwig MG, Seuwen K, Bridges JP. Adhesion GPCR Function in Pulmonary Development and Disease. *Handb Exp Pharmacol*. 2016;234:309–327.

46. Offermanns S, Zhao LP, Gohla A, Sarosi I, Simon MI, Wilkie TM. Embryonic cardiomyocyte hypoplasia and craniofacial defects in G alpha q/G alpha 11-mutant mice. *EMBO J*. 1998;17(15):4304–4312.

47. Wettschureck N, et al. Absence of pressure overload induced myocardial hypertrophy after conditional inactivation of Galphaq/Galpha11 in cardiomyocytes. *Nat Med*. 2001;7(11):1236–1240.

48. Tsilibary EC, Williams MC. Actin and secretion of surfactant. *J Histochem Cytochem*. 1983;31(11):1298–1304.

49. Marino PA, Rooney SA. Surfactant secretion in a newborn rabbit lung slice model. *Biochim Biophys Acta*. 1980;620(3):509–519.

50. Miklavc P, et al. Actin coating and compression of fused secretory vesicles are essential for surfactant secretion--a role for Rho, formins and myosin II. *J Cell Sci*. 2012;125(Pt 11):2765–2774.

51. Tsilibary EC, Williams MC. Actin in peripheral rat lung: S1 labeling and structural changes induced by cytochalasin. *J Histochem Cytochem*. 1983;31(11):1289–1297.

52. Rice WR, Osterhoudt KC, Whitsett JA. Effect of cytochalasins on surfactant release from alveolar type II cells. *Biochim Biophys Acta*. 1984;805(1):12–18.

53. Bates SR, Dodia C, Fisher AB. Surfactant protein A regulates uptake of pulmonary surfactant by lung type II cells on microporous membranes. *Am J Physiol*. 1994;267(6 Pt 1):L753–L760.

54. Muller WJ, Zen K, Fisher AB, Shuman H. Pathways for uptake of fluorescently labeled liposomes by alveolar type II cells in culture. *Am J Physiol*. 1995;269(1 Pt 1):L11–L19.

55. Stevens PA, Wissel H, Zastrow S, Sieger D, Zimmer KP. Surfactant protein A and lipid are internalized via the coated-pit pathway by type II pneumocytes. *Am J Physiol Lung Cell Mol Physiol*. 2001;280(1):L141–L151.

56. Rückert P, Bates SR, Fisher AB. Role of clathrin- and actin-dependent endocytotic pathways in lung phospholipid uptake. *Am J Physiol Lung Cell Mol Physiol*. 2003;284(6):L981–L989.

57. Fukuzawa T, et al. Lung surfactant levels are regulated by Ig-Hepta/GPR116 by monitoring surfactant protein D. *PLoS ONE*. 2013;8(7):e69451.

58. Fisher JH, et al. Pulmonary-specific expression of SP-D corrects pulmonary lipid accumulation in SP-D gene-targeted mice. *Am J Physiol Lung Cell Mol Physiol*. 2000;278(2):L365–L373.

59. Petersen SC, et al. The adhesion GPCR GPR126 has distinct, domain-dependent functions in Schwann cell development mediated by interaction with laminin-211. *Neuron*. 2015;85(4):755–769.

60. Wu J, et al. Differential proteomic analysis of bronchoalveolar lavage fluid in asthmatics following segmental antigen challenge. *Mol Cell Proteomics*. 2005;4(9):1251–1264.

61. John AE, et al. Loss of epithelial Gq and G11 signaling inhibits TGFβ production but promotes IL-33-mediated macrophage polarization and emphysema. *Sci Signal*. 2016;9(451):ra104.

62. Dietl P, Haller T, Frick M. Spatio-temporal aspects, pathways and actions of Ca(2+) in surfactant secreting pulmonary alveolar type II pneumocytes. *Cell Calcium*. 2012;52(3-4):296–302.

63. Frick M, Eschertzhuber S, Haller T, Mair N, Dietl P. Secretion in alveolar type II cells at the interface of constitutive and regulated exocytosis. *Am J Respir Cell Mol Biol*. 2001;25(3):306–315.

64. Tang X, et al. GPR116, an adhesion G-protein-coupled receptor, promotes breast cancer metastasis via the Gαq-p63RhoGEF-Rho GTPase pathway. *Cancer Res*. 2013;73(20):6206–6218.

65. Gonzalez RF, Dobbs LG. Isolation and culture of alveolar epithelial type I and type II cells from rat lungs. *Methods Mol Biol*. 2013;945:145–159.

66. Wang J, et al. Differentiated human alveolar epithelial cells and reversibility of their phenotype in vitro. *Am J Respir Cell Mol Biol*. 2007;36(6):661–668.

67. Ito Y, Correll K, Schiel JA, Finigan JH, Prekeris R, Mason RJ. Lung fibroblasts accelerate wound closure in human alveolar epithelial cells through hepatocyte growth factor/c-Met signaling. *Am J Physiol Lung Cell Mol Physiol*. 2014;307(1):L94–105.

68. Miller WE, Houtz DA, Nelson CD, Kolattukudy PE, Lefkowitz RJ. G-protein-coupled receptor (GPCR) kinase phosphorylation and beta-arrestin recruitment regulate the constitutive signaling activity of the human cytomegalovirus US28 GPCR. *J Biol Chem*.

    2003;278(24):21663–21671.

69. Bligh EG, Dyer WJ. A rapid method of total lipid extraction and purification. *Can J Biochem Physiol.* 1959;37(8):911–917.

70. Mason RJ, Nellenbogen J, Clements JA. Isolation of disaturated phosphatidylcholine with osmium tetroxide. *J Lipid Res.* 1976;17(3):281–284.

71. Ikegami M, Na CL, Korfhagen TR, Whitsett JA. Surfactant protein D influences surfactant ultrastructure and uptake by alveolar type II cells. *Am J Physiol Lung Cell Mol Physiol.* 2005;288(3):L552–L561.